ADVANCED FUNCTIONAL MATERIALS
www.afm-journal.de

Tracking the Endosomal Escape of Nanoparticles in Live Cells Using a Triplex-Forming Oligonucleotide

Sukhvir Kaur Bhangu, Liviana Mummolo, Soraia Fernandes, Alessia Amodio, Agata Radziwon, Brendan Dyett, Marco Savioli, Nitin Mantri, Christina Cortez-Jugo, Frank Caruso, and Francesca Cavalieri**

Nanoparticle-mediated intracellular delivery of oligonucleotides is a complex phenomenon that depends on the architecture and the intracellular trafficking of the engineered nanoparticles. Unravelling the molecular arrangements of oligonucleotides within the nanoparticles as well as their intracellular behavior are essential for designing effective nucleic acid delivery systems. Herein, a simple and general strategy for probing the endosomal escape of nanoparticles carrying oligonucleotides in live cells is reported. A triplex-forming oligonucleotide probe is designed to target the transcription factor, kappa-light-chain-enhancer of activated B cells (NF-κB), in the cytosol of cells and to transduce the binding into a fluorescent Förster resonance energy transfer (FRET) signal. The combined use of the triplex-forming oligonucleotide probe and super-resolution microscopy enables the elucidation of the morphology, intracellular localization, and endosomal escape of the oligonucleotide-loaded nanoparticles on a molecular level and with nanoscale resolution. The co-delivery of the FRET probe and mRNA in cells via lipid- and polymer- based nanoparticles allow simultaneous correlation of the endosomal escape properties of nanoparticles and gene expression efficiency.

1. Introduction

Functional oligonucleotides are promising therapeutic agents to treat cancer, infections, and autoimmune diseases.[1] However, the intracellular delivery of oligonucleotides to cytoplasmic or nuclear targets in the host cell is hindered by various physiological barriers, including low cell membrane permeability, low extracellular and intracellular stability, and undesirable immune responses to nucleic acids. Various approaches have been developed to enable the efficient and safe delivery of oligonucleotides, including the engineering of lipid nanoparticles, nano-sized electrostatic complexes (i.e., polyplexes, and lipoplexes), and inorganic nanoparticles (NPs) (gold, silica, iron oxide, and lanthanide). However, the design of highly efficient carriers remains a major challenge in gene therapy.[1–2] In particular, the translocation of nucleic acid-loaded NPs from the endosomes to the cytosol is highly inefficient (<2%), resulting in the degradation of the cargo in the endocytic vesicles.[3] This is considered the rate-limiting step in gene delivery. This intracellular process, referred to as "endosomal escape", occurs at the nanoscale and the intracellular concentration of the nucleic acid cargo is typically too low (nano-to-picomolar) to be tracked precisely.[4] Through the use of super-resolution microscopy[5] and live cell fluorescence correlation spectroscopy (FCS), we have demonstrated that small-interfering RNA (siRNA) and oligonucleotide molecules can remain stably bound to polyplexes and lipoplexes following endosomal escape.[5a,c] Hence, in addition to inefficient endosomal escape, unpacking nucleic acids from NPs can be a major barrier to the effective transfer of genes to the cytosolic or nuclear targets. These observations highlight the complexity of NP-mediated intracellular delivery of nucleic acids, which depends not only on cellular machinery but also on the morphology and thermodynamic stability of the engineered NP–nucleic acid construct. Therefore, unravelling the molecular arrangements of nucleic acids within the NPs as well as tracking the intracellular behavior of the construct are essential for rationally designing effective gene delivery systems. Equally important is the development of microscopy and biosensing tools for visualizing the

S. K. Bhangu, B. Dyett, N. Mantri, F. Cavalieri
School of Science
RMIT University
Melbourne, Victoria 3000, Australia
E-mail: francesca.cavalieri@rmit.edu.au

S. K. Bhangu, L. Mummolo, S. Fernandes, A. Amodio, A. Radziwon, M. Savioli, C. Cortez-Jugo, F. Caruso
Department of Chemical Engineering
The University of Melbourne
Parkville, Victoria 3010, Australia
E-mail: fcaruso@unimelb.edu.au

M. Savioli, F. Cavalieri
Dipartimento di Scienze e Tecnologie Chimiche
Università degli Studi di Roma "Tor Vergata"
Via della Ricerca Scientifica 1, Rome 00133, Italy

The ORCID identification number(s) for the author(s) of this article can be found under https://doi.org/10.1002/adfm.202311240

DOI: 10.1002/adfm.202311240

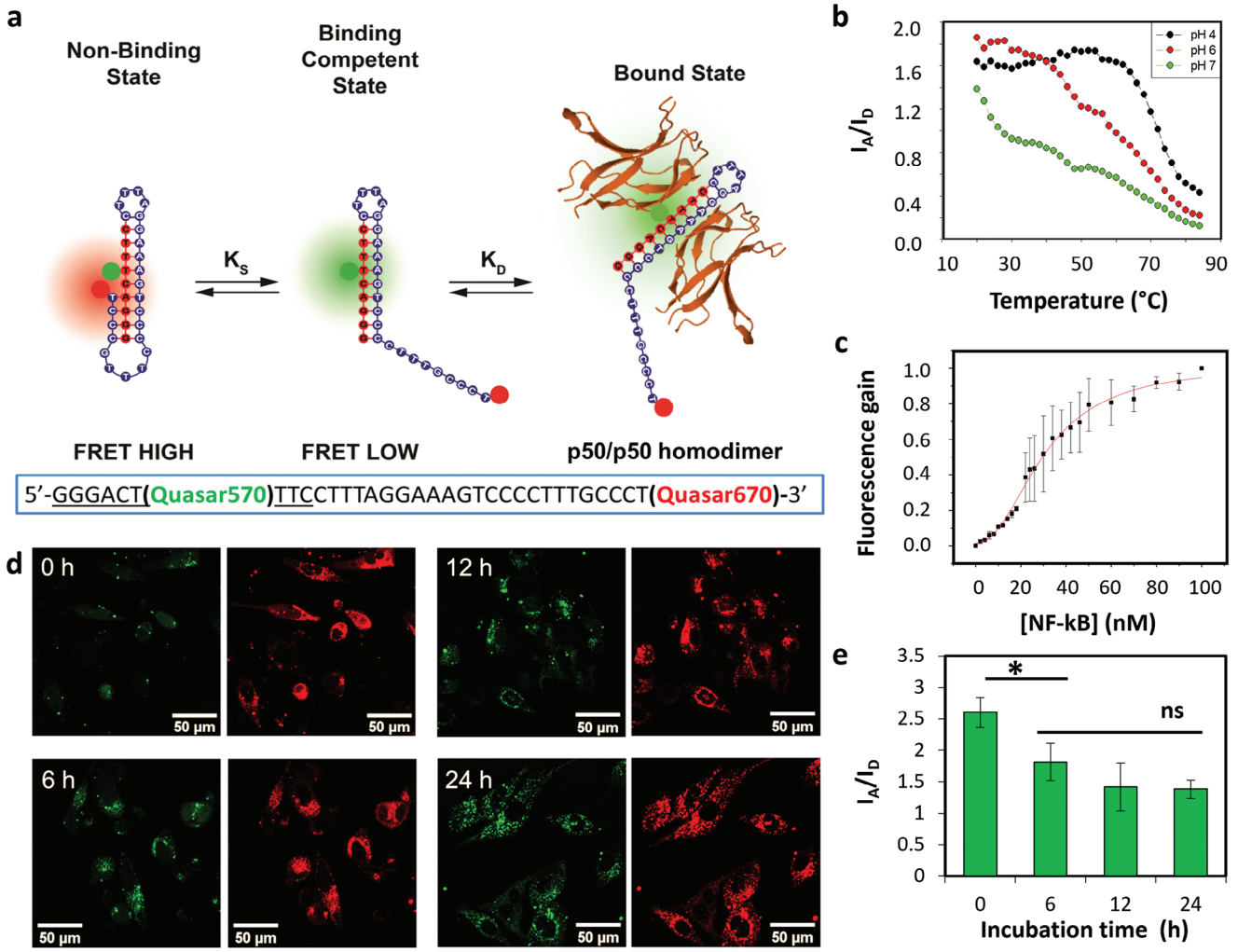

Figure 1. a) Schematic showing ODN_{HT} arranged in triplex and duplex conformations at equilibrium and the binding of ODN_{HT} duplex to NF-κB protein. In the nonbinding triplex conformation, the donor and acceptor are in close proximity ("FRET HIGH"). In the binding duplex conformation, the donor and acceptor are at a larger distance ("FRET LOW"). K_S, switching equilibrium constant; K_D, dissociation constant. The large red and green circles represent Quasar670 (acceptor) and Quasar570 (donor), respectively. b) Melting curves of ODN_{HT} at pH 4, 6, and 7 in 14 mM NaCl, and 10 mM $MgCl_2$. c) Binding curve of ODN_{HT} (5 nM) to NF-κB p50/p50 dimer in PBS (pH 7.4, 37 °C) obtained by plotting the relative increase in fluorescence signal at 570 nm as a function of the concentration of NF-κB. Error bars represent standard deviations, n = 3. d) Confocal microscopy images of live PC3 cells after transfection for 2 h with ODN_{HT} (10 nM) by lipofectamine and further incubation for 0, 6, 12, and 24 h. The donor (Quasar570) was excited at 546 nm, and the emission intensities of the donor (green) and acceptor (Quasar670, red) were imaged and quantified by the spectral profiles. e) Variations in I_A/I_D measured in live PC3 cells in the cytosol as a function of incubation time after transfection with ODN_{HT}. Error bars represent standard deviations, n = 60 cells. $^*p < 0.05$; ns, $p > 0.05$.

endosomal escape of such carriers in live cells and probing the functionality of the released therapeutic cargo with high sensitivity. Endosomal escape probes based on proteins, such as split green fluorescence protein,[6] inactivated Renilla luciferase,[7] and split NanoLuciferase,[8] have been developed for the direct quantification of cytosolic delivery of cargo peptides and nucleic acids. However, these probes have shown limited sensitivity and versatility, as specifically engineered cell lines and chemically modified cargo molecules are required.[7–8]

In the present work, we demonstrate a general strategy for tracking the endosomal escape of lipid- and polymer-based NPs in cells. A triplex-forming oligonucleotide was designed to target the transcription factor, kappa-light-chain-enhancer of activated B cells (NF-κB), in cells and to transduce the recognition of the transcription factor into a variation of a Förster resonance energy transfer (FRET) signal through a binding-induced conformational change. As the NF-κB is a ubiquitous transcription factor, this strategy could be used in diverse cell types. In particular, this approach is useful for studying many cancer cells where the cytoplasmic NF-κB is upregulated and constitutively activated. A DNA nanoswitch with a double stem-loop structure was previously engineered for the intracellular targeting of NF-κB.[5a,b] Although the DNA nanoswitch selectively bound NF-κB in live cells, a portion of the DNA nanoswitch degraded. Compared with the previously engineered double stem-loop nanoswitch, the triplex-forming oligonucleotide engineered

in the present study was more efficient, as it showed a high binding affinity for NF-κB and high resistance against intracellular DNAse. The triplex-forming oligonucleotide was thus examined as a cargo and sensor for probing the endosomal escape of NPs. The approach was first validated in vitro and then in live cells by using lipid-based NPs (i.e., lipofectamine) for the transfection of the oligonucleotide in prostate cancer PC3 cells. We then engineered a non-toxic and biodegradable NP[9] extracted on a large scale from sweet corn,[10] i.e., phytoglycogen (PG), for the intracellular delivery of the NF-κB-binding oligonucleotide. By combining single-molecule super-resolution microscopy and the bioactive triplex-forming oligonucleotide, we investigated the morphology and composition of the oligonucleotide–PG complexes on a single-particle basis, visualized the intracellular localization and endosomal escape of the complex with nanoscale resolution, and finally probed the cytosolic release of the NF-κB-binding oligonucleotide. Finally, we demonstrated that the triplex-forming oligonucleotide can be co-formulated into nanoparticles with mRNA to correlate the endosomal escape properties of nanoparticles and gene expression efficiency in cells.

Overall, this study introduces a versatile tool for tracking the endosomal escape of NPs carrying nucleic acids and highlights the potential of a plant-sourced nanosugar as a carrier for therapeutic nucleic acids such as gapmers, aptamers, and splice-switching antisense oligonucleotides.

2. Results and Discussion

2.1. Engineering a Signaling Oligonucleotide to Track the Endosomal Escape of Nucleic Acid of Nanoparticles

A DNA 33-mer oligonucleotide, hereafter referred to as ODN_{HT}, was designed using an in silico mfold web server to interconvert between a hairpin (H) and an intramolecular triple helix (T) (**Figure 1a**). The first 24 residues fold to form a Watson Crick hairpin duplex with a four-base loop. The 3′-terminal nine-base tail forms a five-base loop and Hoogsteen hydrogen bonds with three guanines (CGC triad) and one adenine (TAT triad) to generate an intramolecular triplex. A donor–acceptor FRET pair (Quasar570–Quasar670) was introduced on T6 and T33 bases, respectively, to probe the triplex–duplex transition by FRET signal. The hairpin was designed to encode the duplex binding sequence for the nuclear factor-kappa B p50/p50 dimer (NF-kB) (5′-GGGACTTTCC-3′, depicted in red in Figure 1a). We hypothesize that the equilibrium between the triplex and duplex conformations in ODN_{HT} can be shifted toward the duplex-binding state upon interaction with NF-κB (Figure 1a).[11] When the ODN_{HT} exists in the intramolecular triplex state, the donor and acceptor are in close proximity and the emission of the donor is efficiently quenched by FRET. In contrast, when the ODN_{HT} exists in the duplex state, the acceptor and donor are at a larger distance with reduced FRET. Hence, by measuring the changes in FRET efficiency, expressed as a ratio of the fluorescence emission intensities of the acceptor and donor (i.e., I_A/I_D), the change in the conformation of ODN_{HT} upon binding to NF-κB can be monitored both in vitro and in live cells. First, the equilibrium between the triplex and duplex conformations in the ODN_{HT} was investigated. Figure S1a,b (Supporting Information) shows that ODN_{HT} exhibited FRET with a stable I_A/I_D of 1.75 in phosphate-buffered saline (PBS) solutions in the presence of salt ($MgCl_2$) and over pH 4–7.5. This result suggests an efficient FRET process along with the pH independence of the triplex–duplex equilibrium at physiological conditions. We noticed that at pH 8 (Figure S1b, Supporting Information) the I_A/I_D decreased from 1.75 to 1.25, likely indicating that ODN_{HT} lost its triplex conformation.

To verify the presence of the triplex conformation, melting curves at different pH and low ionic strength (14 mM NaCl, 10 mM $MgCl_2$) were evaluated. At acidic pH, a melting temperature of ≈70 °C was observed (Figure 1b). Under this acidic condition, the triplex is more stable and the triplex-to-duplex and duplex-to-single strand transitions typically occur at similar temperatures.[12] At pH 6, two melting temperatures were detected for ODN_{HT} at ≈40 and ≈70 °C, corresponding to the melting of the triplex and duplex, respectively. At pH 7 and low ionic strength, the melting of the triplex occurred at room temperature (25 °C). Of note, when 1 × PBS (high concentration of salt) was used, ODN_{HT} showed high thermal stability in the range of pH from 4 to 7, as demonstrated by FRET values which remained constant up to 80 °C. These results indicate that at physiological conditions, ODN_{HT} forms triplex structures, as shown in Figure 1a.

The binding of ODN_{HT} to NF-κB p50/p50 dimer (Figure 1a) was first evaluated in vitro (test tube). With increasing concentrations of NF-κB, the fluorescence emission intensity of the donor at 570 nm gradually increased, whereas that of the acceptor at 658 nm decreased (Figure S2, Supporting Information). This result indicates that the equilibrium between the two states (K_s) is shifted toward the binding duplex state in the presence of NF-κB, as shown in Figure 1a. The binding curves and the relative dissociation constant, K_D, were obtained through titration experiments by monitoring the relative increase in the fluorescence signal of the donor (Figure 1c). By applying the Hill equation, an apparent dissociation constant, K_d, of 25 ± 1 nM was obtained with a Hill coefficient of 2.8, indicating that cooperative binding is involved.[13]

The binding of ODN_{HT} with NF-κB was then studied in live PC3 cells. The NF-κB is a ubiquitous transcription factor present in the cytosol in an inactive form.[14] The cytoplasmic NF-κB is upregulated and constitutively activated in many cancer cells, including prostate cancer PC3 cells, and ultimately translocated into the nucleus.[15] Cells were transfected with ODN_{HT} (10 nM) targeting NF-κB using the commercial transfection agent lipofectamine. A standard and validated transfection protocol using lipofectamine was used to avoid cell toxicity.[5a] After incubation for 2 h, the transfection medium was discarded, and the cells were incubated in fresh culture medium for up to 24 h. The intracellular FRET spectral profiles of ODN_{HT} were acquired by confocal microscopy on live cells. Upon excitation of the donor, I_A/I_D was monitored in at least 30 cells in the cytosol region at different time points (2–24 h) (Figure 1d). After 2 h of transfection (corresponding to an incubation time of 0 h), the average I_A/I_D value of the cells was 2.5. The high FRET value is consistent with the arrangement of ODN_{HT} into a triplex conformation. In addition, the FRET value obtained in live cells was higher than the value obtained in the test tube experiment in PBS (FRET 1.8).

Table 1. Diffusion coefficient (D) values of ODN_{HT} in PBS and live cells transfected with 50 nM ODN_{HT} for 4 h and analyzed after a 24-h incubation period. The ODN_{HT} in solution or inside cells was excited using a 561 nm laser and signals were detected using a 600/50 bandpass filter.

	D [μm^2 s^{-1}]	
	PBS pH 7.4	Cell cytosol
ODN_{HT}	100 ± 2	81 ± 10, 7.5 ± 0.8[a)]
ODN_{HT} degraded by DNAse	238 ± 50	–

[a)] Fast and slow diffusing species were observed in the region of interest in the cytosol of cells.

This may be attributed to either variation of the quantum yield of the donor and acceptor in live cells or intracellular crowding effects that can promote the stabilization of the triplex conformation. An overall progressive decrease in I_A/I_D was observed with increasing incubation time, with a leveling off observed after 12 h (Figure 1e). The overall reduction in I_A/I_D with increasing incubation time may indicate either the binding of ODN_{HT} to the target transcription factor in the cytosol or the degradation of ODN_{HT} in the endo-lysosomal compartments. Interestingly, confocal microscopy images (Figure 1d) acquired at incubation times 6–24 h show that ODN_{HT} primarily localizes in the cytosol, indicating that the ODN_{HT}/NF-κB complex is unable to translocate to the nucleus. However, a transient nuclear signal in live cells was observed after 2 h transfection where the I_A/I_D value was 1.7 (Figure S3, Supporting Information). This may indicate that the released ODN_{HT} can also bind to the activated cytosolic NF-κB and translocate in the nucleus or first diffuse into the nucleus and then bind to the activated nuclear NF-κB. It is known that NF-κB is shuttled to the nucleus, and the binding of the NF-κB to its gene targets generally results in the transcription and synthesis of IκB protein. This protein promptly recognizes the NF-κB dimers and re-shuttles them back to the cytosol. This may explain the observed transient localization of fluorescent signal in the nuclei and the disappearance of the signal may indicate that the nuclear ODN_{HT}/NF-κB complex can be actively relocated in the cytosol.

To assess whether ODN_{HT} was degraded while undergoing intracellular trafficking, the diffusion properties of ODN_{HT} (50 nM) were analyzed after lipofectamine-mediated transfection in live cells by FCS (**Table 1**). Specifically, Table 1 shows the measured diffusion coefficient (D) values for ODN_{HT} in PBS solution and live cells, as well as in PBS after treatment with DNAse (1 h, 37 °C). The intact and degraded ODN_{HT} in PBS solution showed D values of 100 ± 2 and 238 ± 50 μm^2 s^{-1}, respectively. Mono-exponential autocorrelation curves were systematically observed in live cells corresponding to the diffusion of one species with D of 81 ± 10 μm^2 s^{-1} after incubation with ODN_{HT} for 24 h. This value is comparable to the D of the sample in PBS, indicating that ODN_{HT} delivered in the cytosol is resistant to intracellular degradation. We also observed another slow diffusing species with D of 7.5 ± 0.8 μm^2 s^{-1}, which was ascribed to either ODN_{HT}–lipofectamine or ODN_{HT}–NF-κB nano complexes (NCs) localized in the cytosol; FCS analysis does not allow differentiation between these two diffusing species. In our work in 2020,[5a] we reported that a negative scrambled control FRET hairpin oligonucleotide lacking the NF-κB binding domain typically showed limited specific binding to NF-κB p50/p50 or p50/p65 dimers in a test tube. The intracellular FRET studies performed on PC3 cells transfected with the negative control FRET hairpin oligonucleotide revealed no variations in FRET values as a function of incubation time and limited colocalization with NF-κB by immunostaining and microscopy studies.

Overall, the FRET microscopy and FCS studies performed on live cells indicate that the ODN_{HT} designed in the present work can be effectively delivered intact in the cells, and binding to the target cytosolic NF-κB is transduced into a FRET signal variation.

2.2. Determining the Molecular Architecture of ODN_{HT}–Nano sugar Nano complexes

The FRET ODN_{HT} was employed as a model system of therapeutic oligonucleotides to study the architecture of oligonucleotide–glycogen constructs and probe the mechanism of intracellular delivery of oligonucleotides. As the target protein NF-κB is produced in the cytosol, the analysis of the FRET signal arising from the intracellular ODN_{HT} enables probing of the endosomal escape of ODN_{HT} from oligonucleotide–phytoglycogen constructs. PG nanoparticles, PG NPs, are naturally occurring nanoparticles derived from sweet corn with a dendrimer-like structure composed of repeating units of glucose connected by linear α-D-(1–4) glycosidic linkages with α-D-(1–6) branching.[16] PG NPs have hydrodynamic diameters of ≈80 ± 30 nm (Figure S4a, Supporting Information) and a neutral ζ-potential value of −1 ± 2 mV, as determined by dynamic light scattering (DLS) and electrophoretic mobility measurements.

As determined from the static light scattering measurements, the molecular weight of the PG NPs was 18 ± 2 MDa (Figure S5, Supporting Information). Cryo-transmission electron microscopy (cryo-TEM) images revealed the cauliflower-like appearance morphology of PG NPs in aqueous solution (Figure S6a, Supporting Information), with a number mean diameter D_n of 55 ± 13 nm (Figure S6b, Supporting Information), in agreement with the DLS data (number size distribution, Figure S4a, Supporting Information). To enable the complexation of ODN_{HT}, positively charged PG NPs, hereafter referred to as PG_{EDA} NPs, were synthesized by introducing ethylenediamine (EDA) groups on the polysaccharide scaffold through a reductive amination reaction (Scheme S1, Supporting Information). The substitution degree with EDA was determined by ^{1}H-NMR analysis of the PG_{EDA} NP suspension (Figure S7 and Table S1, Supporting Information). The integration of the NMR peaks indicated a substitution degree of ≈19%. The measured ζ-potential and hydrodynamic diameter of the PG_{EDA} NPs were 41 ± 7 mV and 93 ± 35 nm (polydispersity index (PDI) = 0.2), respectively, indicating the effective surface modification of the PG NPs (Figure S3b, Supporting Information). PG_{EDA} NPs maintained a cauliflower morphology following chemical modification, as shown in the representative cryo-TEM image in **Figure 2a**, with a D_n of 55 nm (Figure 2b).

The unmodified PG NPs were effectively degraded by α-amylase to up to 90% within 24 h, whereas PG_{EDA} NPs showed higher resistance to α-amylase digestion (30% degradation only) after a similar treatment (Figure 2c). In our earlier study,[17] the

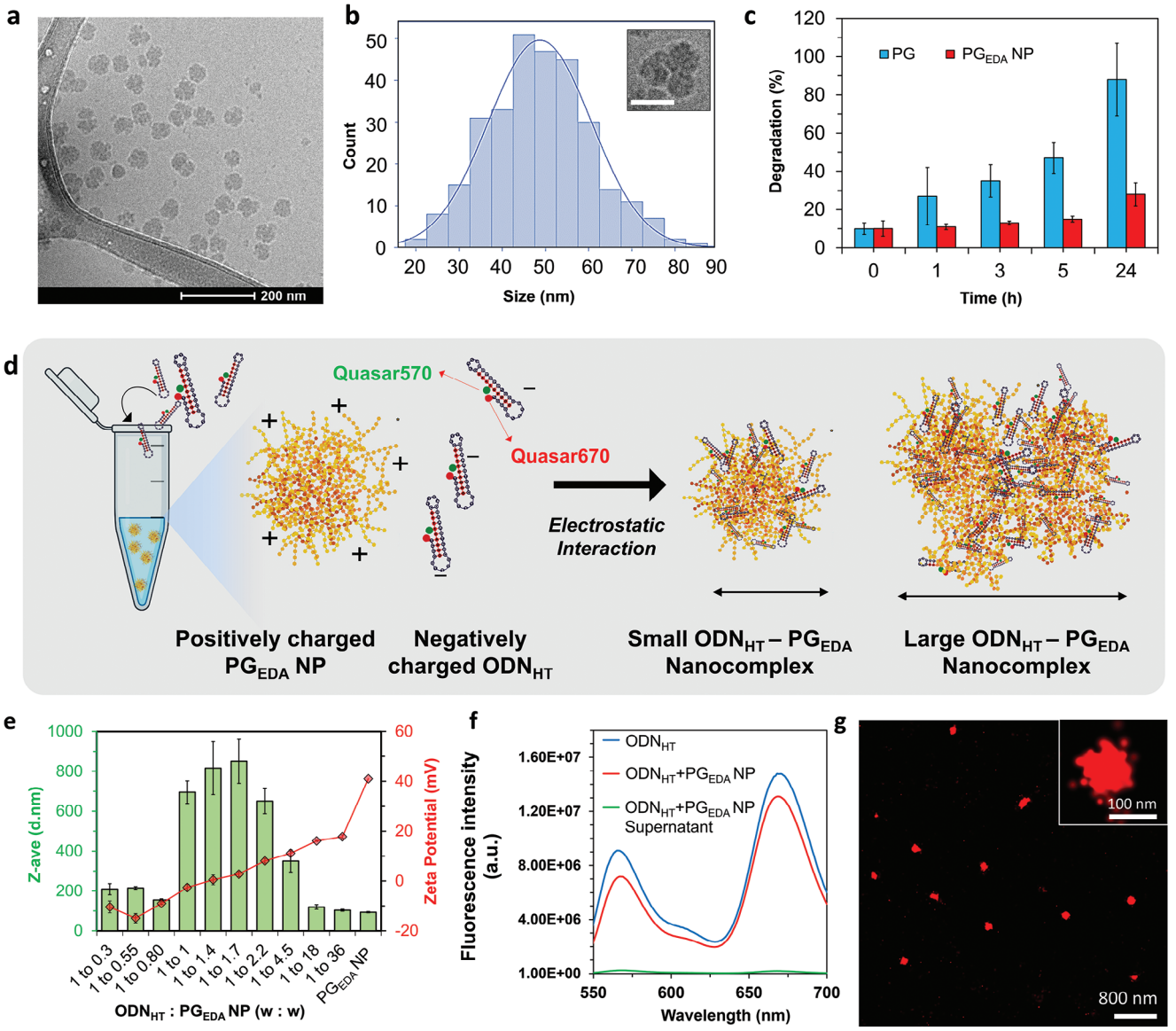

Figure 2. a) Cryo-TEM image and b) number size distribution of PG_{EDA} NPs. The inset in (b) shows a cryo-TEM image of a single PG_{EDA} NP, scale bar 50 nm. c) Comparison of the degradability of unmodified PG NPs and PG_{EDA} NPs by α-amylase. The extent of degradation of the PG-based particles by α-amylase as a function of time was determined using the Somogyi–Nelson assay. d) Schematic showing the complexation between a positively charged PG_{EDA} NP and negatively charged ODN_{HT}. e) Size and ζ-potential of complexes prepared at different ODN_{HT}-to-PG_{EDA} NP ratios. f) Fluorescence emission spectra of ODN_{HT}, and ODN_{HT}–PG_{EDA} NC (prepared at a ratio of 1:36) and its supernatant, suggesting binding of ODN_{HT} to PG_{EDA} NPs (λ_{ex} = 520 nm). g) Representative dSTORM microscopy image of AF647-labeled PG_{EDA} NPs in the hydrated state after deposition on a glass slide.

limited degradability displayed by amine-functionalized glycogen NPs was attributed to the electrostatic repulsion between the cationic glycogen NPs and the positively charged enzymes (isoelectric point = 6.5–7). These results further confirm our hypothesis and suggest that PG_{EDA} NPs are not readily degraded in biological environments containing α-amylase (i.e., blood, gastrointestinal tract). The interaction between the cationic PG_{EDA} NPs and negatively charged ODN_{HT} to form the nano complex ODN_{HT}–PG_{EDA} NC is driven by electrostatic interactions (Figure 2d) and likely by an increase in entropy owing to the release of counterions and coordinated water molecules. However, it is essential to optimize the ODN_{HT}-to-PG_{EDA} NP weight ratio to efficiently load the desired amount of ODN_{HT} molecules into PG_{EDA} NPs and avoid the uncontrolled formation of large aggregates to ultimately fine-tune the nanoscale structure of the complex. The morphology of ODN_{HT}–PG_{EDA} NC was tailored by varying the ODN_{HT}-to-PG_{EDA} NP weight ratio (from 1:0.3 to 1:36) during preparation. The size and ζ-potential of the obtained complexes were determined (Figure 2e). At increasing ratios from 1:0.3 to 1:0.8 w/w, ODN_{HT} molecules interacted with PG_{EDA} NPs to form stable nanocomplexes of 150–200 nm in size with a negative ζ-potential (ranging from −10 to −15 mV). When ODN_{HT} and PG_{EDA} NPs were mixed at increasing ratios ranging from 1:1 to 1:4.5, submicron polydisperse aggregates (300–900 nm)

with a neutral ζ-potential formed, suggesting that the neutralization of positive charges exposed on PG_{EDA} NPs by ODN_{HT} induces clustering of the PG_{EDA} NPs. Finally, at the higher ratios (from 1:18 to 1:36), the larger aggregates disassembled to form well-dispersed nanocomplexes, with a diameter of ≈100 nm (PDI = 0.25) and a ζ-potential of 18 ± 5 mV (Figure 2e). It is worth noting that at the higher ratios, excess free PG_{EDA} NPs may be also present, therefore, the DLS technique probes the hydrodynamic diameters of both ODN_{HT}–PG_{EDA} NC and free PG_{EDA} NPs. Nano complexation obtained at the weight ratios of 1:18 and 1:36 corresponds to 88 and 44 ODN_{HT} molecules per NP, respectively. The fluorescence emission spectra of ODN_{HT}–PG_{EDA} NCs (prepared at a ratio of 1:36) after purification and its supernatant solution confirmed that all ODN_{HT} were incorporated into PG_{EDA} NPs (Figure 2f) and, more importantly, maintained the high FRET triplex conformation upon assembly.

To gain deeper insights into the size and architecture of the nano complexes at the molecular level, the structure and morphology of the nano complexes were investigated by stochastic optical reconstruction microscopy (STORM). This technique, which is based on single-molecule localizations detected during imaging, allows the investigation of the equilibrium of complexation and individual nano complexes with nanometer resolution. The ODN_{HT}–PG_{EDA} NCs were first prepared using non-labeled PG_{EDA} NPs and the FRET ODN_{HT} at different ODN_{HT}-to-PG_{EDA} weight ratios. The nano complexes were then deposited on a glass coverslip for dSTORM-imaging using the Total Internal Reflection Fluorescence (TIRF). The molecule localizations were analyzed to quantitatively estimate the size of the nanocomplexes and the number of localizations inside single nanocomplexes. Each ODN_{HT} molecule carries a photo-switchable fluorophore, Quasar670 (Figure S8, Supporting Information), hence the number of detected localizations is proportional to the number of ODN_{HT} molecules embedded in the nanocomplex. As a control, Alex Fluor 647 (AF647)-labeled PG_{EDA} NPs (Figure 2g) were also deposited on a glass coverslip and imaged by *d*STORM to compare the size of the NPs before and after complexation with ODN_{HT}. As seen in Figure S9 (Supporting Information), the adsorbed PG_{EDA} NPs displayed a size distribution with a peak at 50 nm, which is in agreement with the size distribution obtained by cryo-TEM imaging.

Figure 3a1–a4 shows representative dSTORM images of the ODN_{HT}–PG_{EDA} NCs obtained at different ODN_{HT}-to-PG_{EDA} NP ratios. The diameter of the nano complexes was quantified and plotted on a frequency histogram, as shown in Figure 3b1–b4. Unlike DLS, STORM analysis enables probing only the size of ODN_{HT}–PG_{EDA} NCs as we used non-labeled PG_{EDA} NPs for the complexation. At the weight ratios of 1:4.5 (Figure 3a1) and 1:9 (Figure 3a2), a large amount of signal in the background corresponding to free (non-clustered) ODN_{HT} molecules was observed along with a few nanoclusters of 171 ± 70 nm (Figure 3b1) and 150 ± 50 nm (Figure 3b2) in size, respectively. These results indicate that a limited amount of ODN_{HT} was complexed to PG_{EDA} NPs. Increasing the ratio to 1:18 (Figure 3a3) and 1:36 (Figure 3a4) resulted in the gradual disappearance of free ODN_{HT} molecules and the appearance of spherical nanoclusters of 200 ± 70 nm (Figure 3b3) and 144 ± 70 nm (Figure 3b4) in size, respectively, indicating that all ODN_{HT} molecules were complexed to one or more PG_{EDA} NPs. These results indicate that the efficient condensation of the ODN_{HT} molecules requires an optimal ODN_{HT}-to-PG_{EDA} NP weight ratio of 1:36, which agrees with the fluorescence spectroscopy data (Figure 2f). Scatter plots of the number of localizations as a function of the diameter of the imaged ODN_{HT}–PG_{EDA} NCs (Figure 3c1–c4) confirmed that fewer ODN_{HT} molecules were clustered into ODN_{HT}–PG_{EDA} NCs at the lower ratios of 1:4.5 and 1:9 (Figure 3c1,c2, maximum 250–300 localizations) than at the higher ratios of 1:18 and 1:36 (Figure 3c3,c4, maximum 800 localizations). Furthermore, Figure 3c shows that the number of localizations, which is proportional to the number of ODN_{HT} molecules, increased with the diameter of the nanocomplex. However, a considerable increase in the number of localizations combined with the heterogenous density of the ODN_{HT} molecules ranging from 50 to 800 was observed in the larger (150–200 nm) nano complexes. We hypothesize that the ODN_{HT}–PG_{EDA} NCs can adopt two different morphologies as shown in Figure 2d. Individual PG_{EDA} NPs can either accommodate ODN_{HT} molecules on their brushed surface with limited loading capacity or form larger but uniform nano complexes incorporating many ODN_{HT} molecules and multiple PG_{EDA} NPs. The latter morphology is predominant and ensures that the ODN_{HT} molecules are shielded within the nanocomplex and thus less amenable to DNAse degradation.

These results highlight the potential of STORM microscopy to unveil the molecular structure of multicomponent nanocomplexes as a function of the stoichiometries used by providing qualitative and quantitative information about the number of cargo molecules incorporated in the nanocomplexes. For the subsequent studies and characterization, we selected ODN_{HT}–PG_{EDA} NC obtained at an ODN_{HT}-to-PG_{EDA} NP weight ratio of 1:36 because of its optimal hydrodynamic diameter (105 ± 35 nm) and high ODN_{HT} loading capacity (Figure 2f). The spherical morphologies of the ODN_{HT}–PG_{EDA} NCs and PG_{EDA} NPs were retained in a dry state as confirmed by TEM (Figure S10, Supporting Information). The size distribution of dry particles (39 ± 10 nm) suggests that both the nanocomplexes and PG_{EDA} NP undergo a significant shrinkage upon air drying. This is consistent with the high-water content of PG NPs. Due to the dendrimer-like structure, PG NP is a highly hydrated polysaccharide nanoparticle (23 water molecules per glucose monomer containing a mass of water that is equal to ≈250% of its dry mass).[18]

2.3. Tracking Endosomal Escape of ODN_{HT}–PG_{EDA} NC and Targeting of Cytosolic NF-κB

As the mechanisms involved in the intracellular trafficking of ODN_{HT}–PG_{EDA} NCs strongly influence the delivery of bioactive oligonucleotides, we investigated the endo-lysosomal sequestration and escape of the nanocomplex. First, the cytotoxicity of the ODN_{HT}–PG_{EDA} NCs was investigated. As observed from Figure S11 (Supporting Information), the ODN_{HT}–PG_{EDA} NCs did not cause any toxicity to PC3 prostate cancer cells at any of the concentrations examined (0.1–6 mg mL^{-1}) even after incubation for 48 h. The transfection efficiency of the ODN_{HT}–PG_{EDA} NCs was then examined by transfecting PC3 cells with the nano complex containing 50 nM ODN_{HT} for 2 h (pulse time) and washed with 1 × PBS to remove the non-internalized ODN_{HT}–PG_{EDA} NCs, Subsequently, cells were further incubated for 3, 7, 22, and 46 h

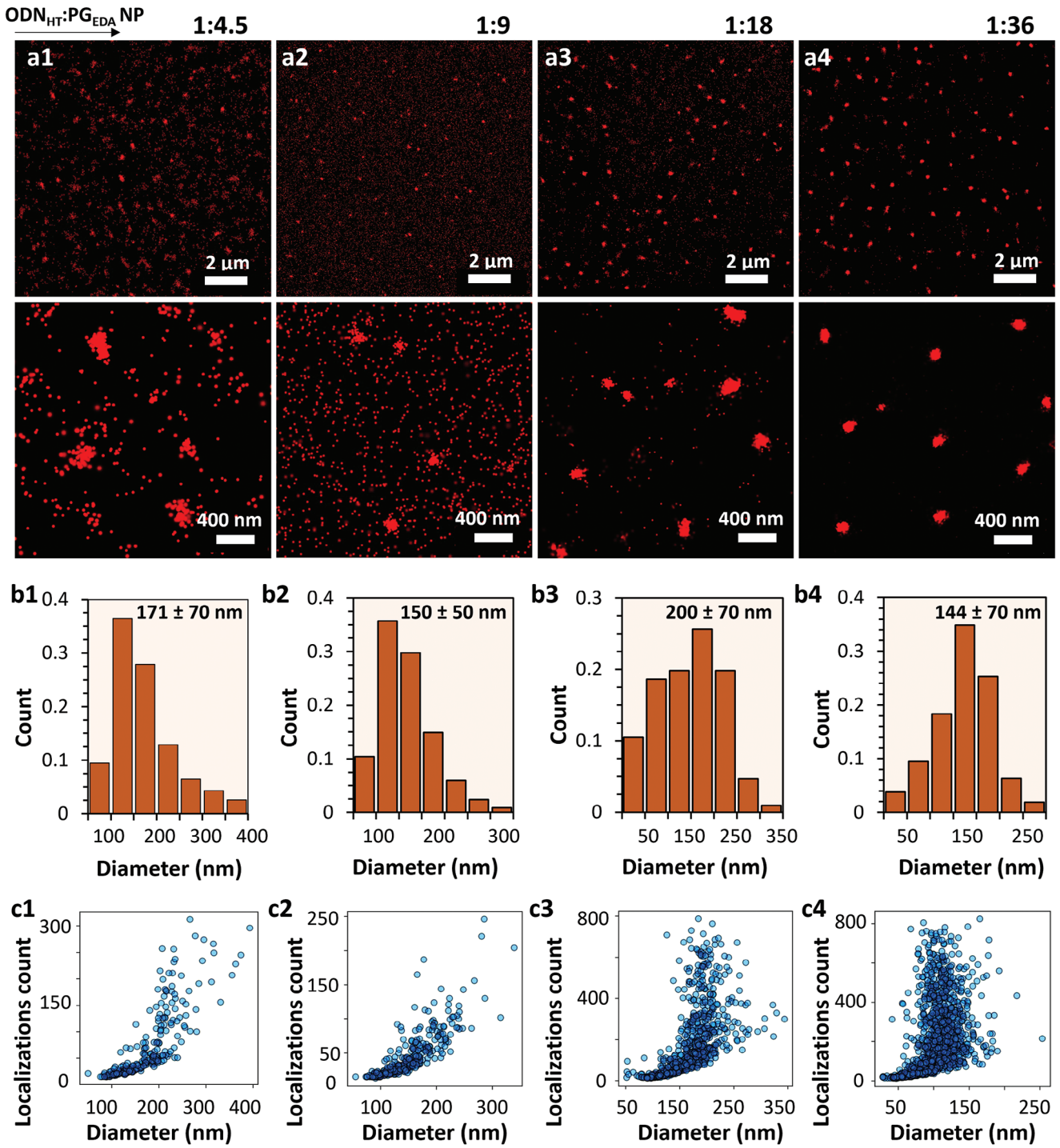

Figure 3. a) dSTORM images and b) size distributions of ODN$_{HT}$–PG$_{EDA}$ NCs at different ODN$_{HT}$-to-PG$_{EDA}$ NP ratios. c) Scatter plots of the number of localizations as a function of the size of nano complexes at different ratios. The weight ratios examined are 1:4.5 (a1–c), 1:9 (a2–c2), 1:18 (a3–c3), and 1:36 (a4–c4).

and analyzed. **Figure** 4a–c shows confocal microscopy images of fixed PC3 cells after incubation with ODN$_{HT}$–PG$_{EDA}$ NCs (red) and immunostaining of early endosomes, late endosomes, and lysosomes (green). The ODN$_{HT}$–PG$_{EDA}$ NCs remained associated with the cell membrane (Figure 4a–c) at the early stage of incubation (2 h) but cellular internalization of the nanocomplexes became apparent as incubation was prolonged. Colocalization analysis of signals (assessed by Pearson correlation coefficient (PCC)) suggested minimal colocalization of the ODN$_{HT}$–PG$_{EDA}$ NC (red) with the early endosomes (green) at all incubation

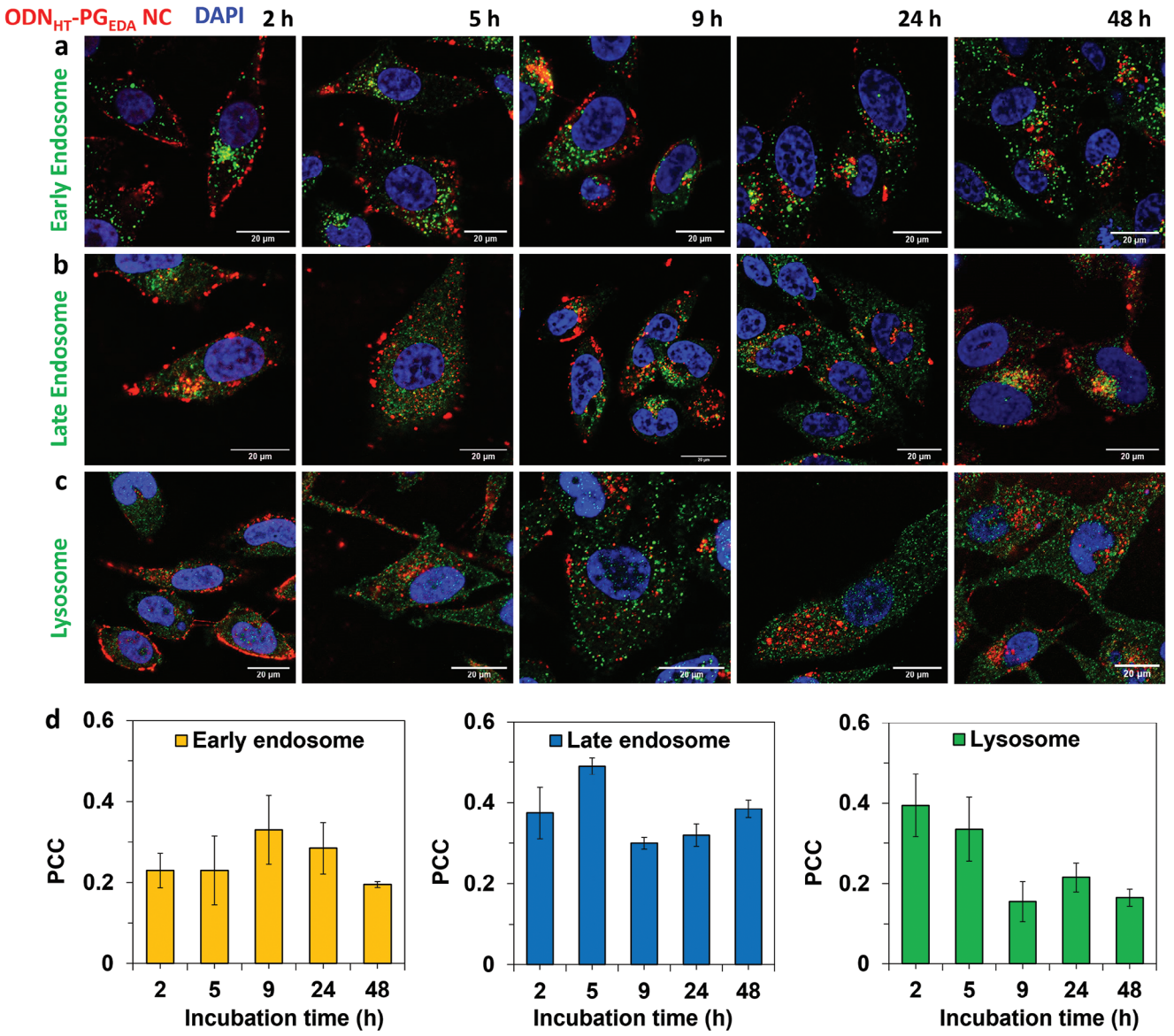

Figure 4. Intracellular trafficking of ODN$_{HT}$–PG$_{EDA}$ NCs (red) when incubated with PC3 cells for 2, 5, 9, 24, and 48 h. Cells were stained for a) early endosomes, b) late endosomes, and c) lysosomes using EEA-1, Rab7, and rabbit lysosomal-associated membrane protein 1 (LAMP-1) antibodies (green), respectively. d) Colocalization of ODN$_{HT}$–PG$_{EDA}$ NCs with early and late endosomes, and lysosomes as a function of incubation time, as assessed by PCC analyses.

times examined (Figure 4d, PCC 0.2–0.3) and partial colocalization with both late endosome (PCC 0.4–0.5) and lysosome (PCC 0.4–0.2) compartments after incubation for ≥5 h (Figure 4d–f). These results indicate ODN$_{HT}$–PG$_{EDA}$ NCs are trafficked from early to late endosomes in the first 5 h and suggest that some ODN$_{HT}$-PG$_{EDA}$ NCs escape from endo-lysosomes. The multicolor STORM microscopy (activator-reporter pair method) study further suggested that the endosomal escape of ODN$_{HT}$–PG$_{EDA}$ NCs occurred within 5–9 h of incubation when individual ODN$_{HT}$–PG$_{EDA}$ NCs (red) were found to be non-colocalized with late endosomes and lysosomes (Figure S12, Supporting Information). Of note, ODN$_{HT}$ is equipped with an activator–reporter FRET pair that enables multichannel acquisition on the microscope.

It is believed that the endosomal escape of ODN$_{HT}$–PG$_{EDA}$ NCs is likely triggered by the proton sponge effect as the secondary amines in EDA exhibit buffering properties and possess pK_a within the range of endosomal pH.[17] This hypothesis was confirmed through potentiometric titration studies, which revealed that, unlike unmodified glycogen,[5c,17] PG$_{EDA}$ NPs exhibit buffering capacity at pH ≈6–7, with a pK_a of ≈6.4 (Figure S13, Supporting Information).

Having verified that ODN$_{HT}$–PG$_{EDA}$ NC can access the cytosol, we assessed the binding of the deployed ODN$_{HT}$ to the NF-κB transcription factor in the cytosol. The intracellular binding of ODN$_{HT}$ to NF-κB protein was probed through FRET measurements. Therefore, PC3 cells were incubated with

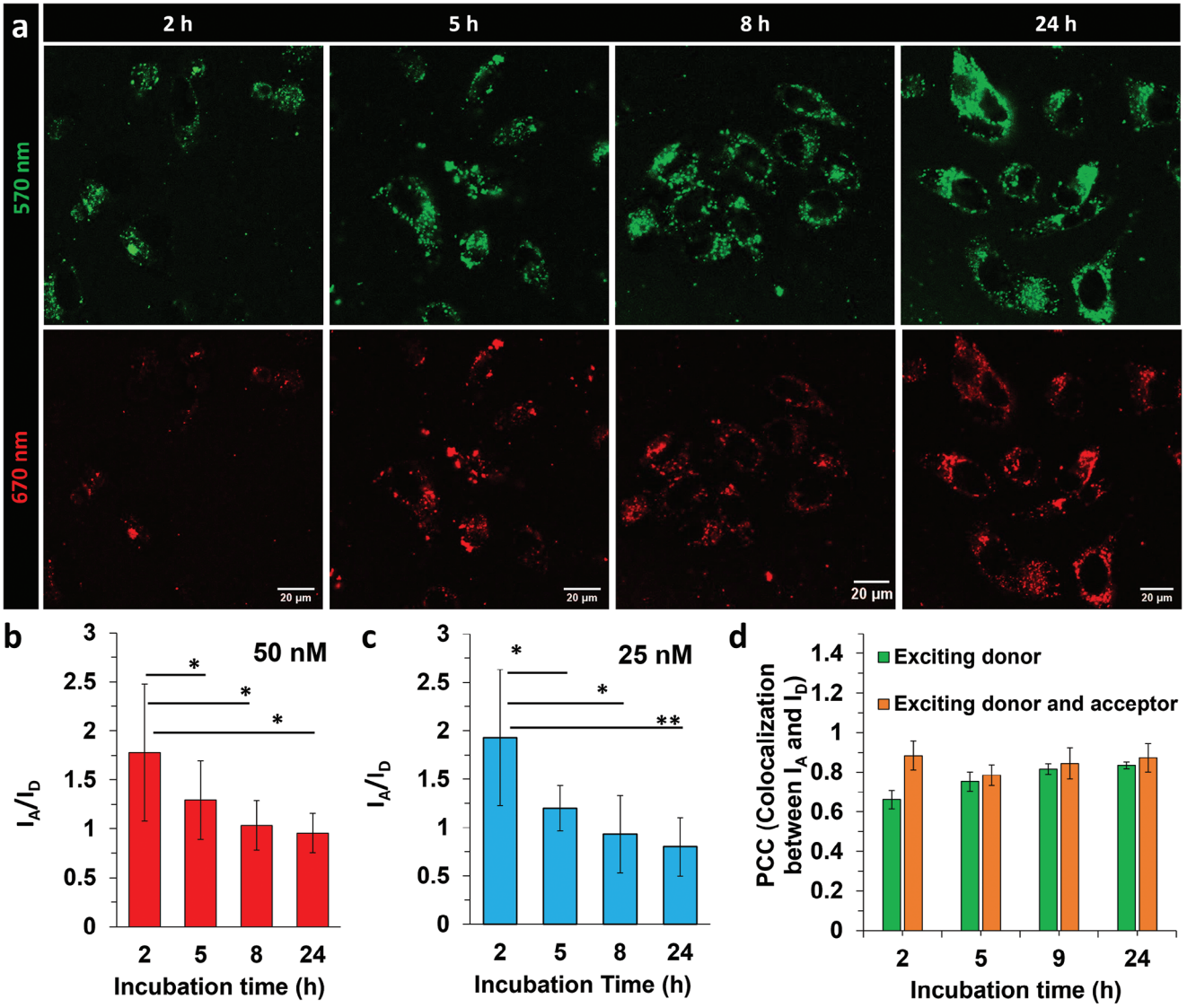

Figure 5. a) Confocal microscopy images of live PC3 cells incubated with ODN_{HT}–PG_{EDA} NCs (prepared at a ratio of 1:36) containing 50 nM DNA for 2 h, followed by washing and further incubation for 3, 6, and 22 h. Laser excitation = 546 nm. b,c) Changes in I_A/I_D in live PC3 cells as a function of incubation time. The signal was acquired in the cytosol in live PC3 cells exposed to ODN_{HT}–PG_{EDA} NCs containing 50 or 25 nM ODN_{HT}. $^{*}p < 0.05$; $^{**}p < 0.01$. d) Colocalization of donor and acceptor emissions as a function of time, as evaluated by PCC.

ODN_{HT}–PG_{EDA} NCs with a payload of 25 or 50 nM ODN_{HT}. Upon excitation of the donor, I_A/I_D was monitored over time in the cytosol (**Figure** 5a). The average signals after 2 h of transfection with 50 and 25 nM ODN_{HT} were 1.7 and 2.0, respectively (Figure 5b,c), which indicates that ODN_{HT} is assembled in triplex conformation at the early stage of incubation. This was also observed when lipofectamine was used as the transfection agent. A gradual decrease in I_A/I_D to 0.8–1.0 was observed as the incubation time increased within a 24 h incubation period. This gradual decrease likely indicates that ODN_{HT} undergoes a conformational transition likely induced upon association with NF-κB protein in the cytosol within a 24 h incubation period. To rule out degradation of the oligonucleotide as a cause for the change observed in I_A/I_D, we evaluated the extent of spatial colocalization of the donor and acceptor emission signals at two experimental conditions (Figure 5d). When excited at 546 nm, the acceptor emission signal was associated with the nondegraded ODN_{HT}, whereas the donor emission could arise from both the degraded and nondegraded ODN_{HT}. A signal colocalization value of 80%–90% indicates that the donor and acceptor are primarily linked together. Similarly, when the donor and acceptor were excited separately using the excitation at 546 and 647 nm, signal colocalization was 90%, indicating that the two fluorophores are spatially close. Overall, Figure 5d shows that the fluorescence signals of the donor and acceptor were spatially colocalized inside the cells, suggesting limited intracellular degradation of ODN_{HT} within the 24 h incubation period examined.

To directly visualize the intracellular association of ODN_{HT} to cytosolic NF-κB, we performed colocalization studies by

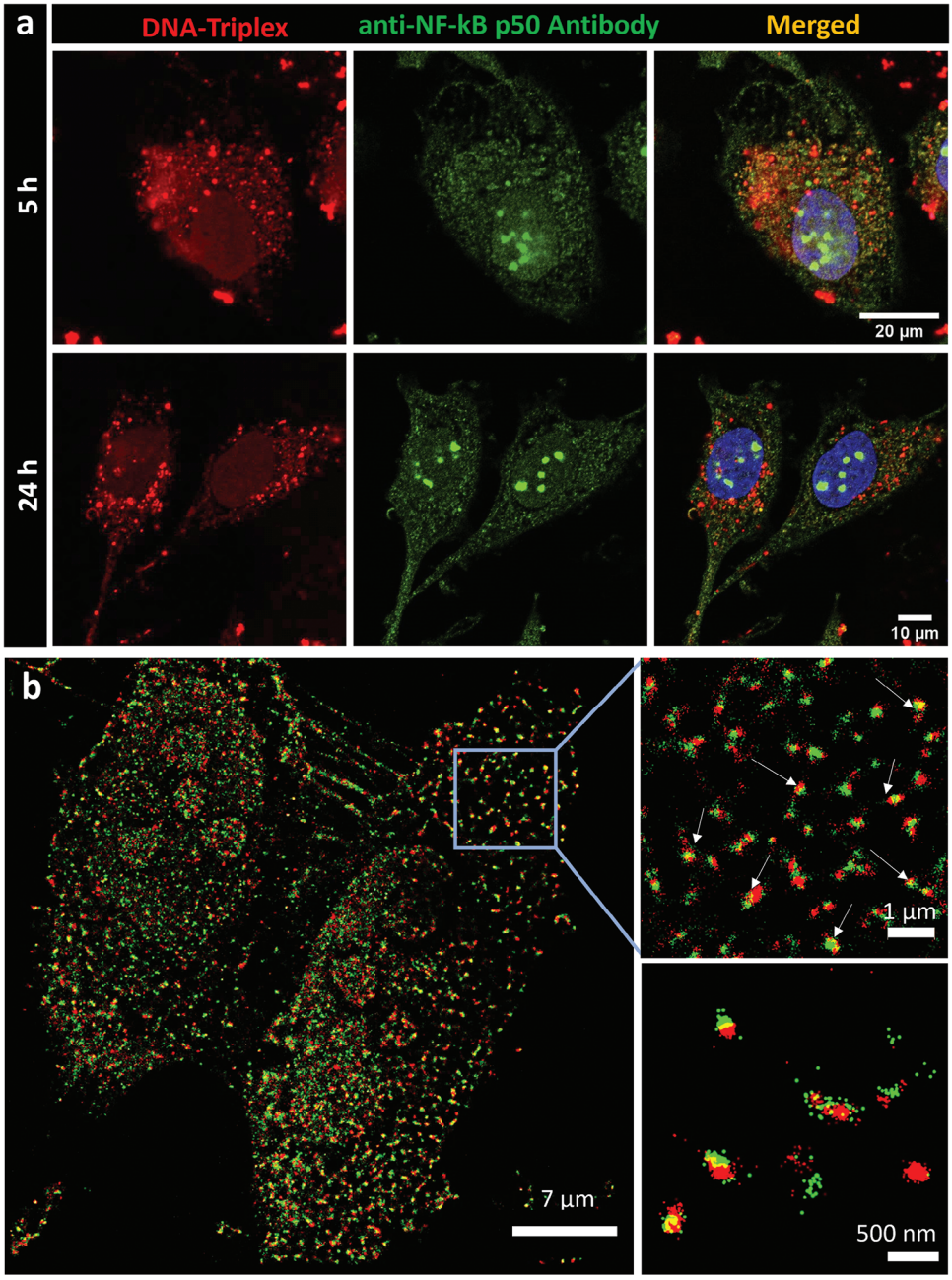

Figure 6. a) Confocal microscopy images of PC3 cells incubated with ODN_{HT}–PG_{EDA} NCs (containing 50 nM ODN_{HT}, red) and stained with AF488-labeled anti-NF-κB p50 antibody (green) post-fixation. b) Multicolor STORM images of ODN_{HT}–PG_{EDA} NCs containing Quasar570 and Quasar670 dyes (red) and NF-κB protein stained with anti-NF-κB p50 antibody dual labeled with AF488 and AF647 (green).

combining STORM and confocal microscopy. Representative confocal images of fixed PC3 cells after 5 and 24 h treatment with ODN_{HT}–PG_{EDA} NCs (50 nM ODN_{HT}) (red) and staining with anti-NF-κB p50 antibody (green) are shown in **Figures** 6a and S14 (Supporting Information). The PCC values obtained from the images acquired after 5 and 24 h incubation were 0.4 and 0.6 (whole cell), respectively, suggesting effective binding of the cytosolic ODN_{HT} to NF-κB. 2D STORM multicolor (activator-reporter pair method) imaging of PC3 cells treated with ODN_{HT}–PG_{EDA} NCs for 24 h was also used to confirm the targeting of ODN_{HT} to NF-κB with nanometer resolution. The NF-κB p50 dimers were imaged using a primary polyclonal anti-NF-κB antibody combined with an AF488/AF647 dual-labeled secondary antibody. Representative STORM images (Figure 6b; Figure S15, Supporting Information) revealed the presence of numerous colocalized assemblies, indicated with arrows, which arise from the effective association of ODN_{HT} to NF-κB. Collectively, these complementary microscopy studies confirm the PG_{EDA} NP-mediated intracellular delivery of oligonucleotides to target cytosolic NF-κB protein.

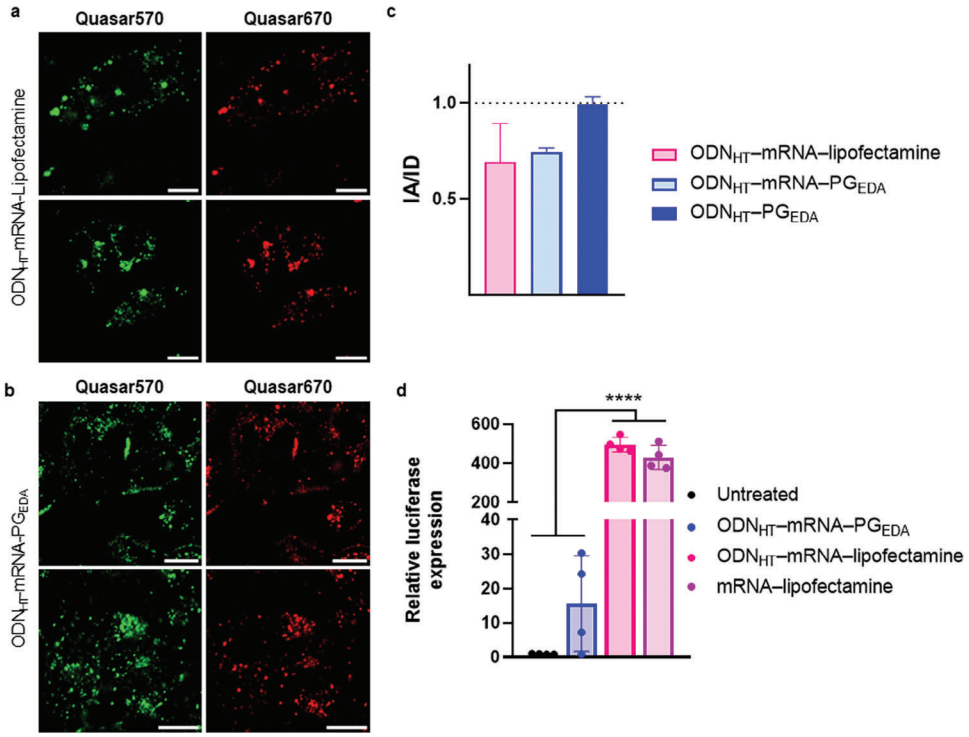

Figure 7. Representative confocal microscopy images of live PC3 cells acquired 24 h post-transfection with a) ODN$_{HT}$–mRNA-lipofectamine and b) ODN$_{HT}$–mRNA-PG$_{EDA}$ NCs (10 nM ODN$_{HT}$, 1 μg mRNA-Luc. The donor was excited at 546 nm, and the emission intensities of the donor (Quasar570, green) and acceptor (Quasar670, red) were imaged and quantified by the spectral profiles. Scale bars: 20 nm. Upper and lower images in the same panel represent repeats of the same measurement. c) I_A/I_D signal quantification 24 h after transfection with ODN$_{HT}$–mRNA-lipofectamine, ODN$_{HT}$–mRNA-PG$_{EDA}$ NCs and ODN$_{HT}$–NCs. d) Relative luciferase expression, normalized to untreated PC3 cells, measured by luminescence after transfection by ODN$_{HT}$–mRNA-PG$_{EDA}$ NCs (50 nM ODN$_{HT}$, 1 μg mRNA-Luc), ODN$_{HT}$–mRNA-lipofectamine (10 nM ODN$_{HT}$, 1 μg mRNA-Luc) and mRNA-lipofectamine (1 μg mRNA-Luc). Statistical analysis was performed by one-way ANOVA (**** $p < 0.0001$).

2.4. Co-Delivery of ODN$_{HT}$ and mRNA Through Nanoparticles Enabled Direct Correlation of Endosomal Escape and Gene Expression Efficiencies

To investigate the versatility of the developed system and methodology and establish a correlation between endosomal escape of nanoparticles and the efficiency of gene expression, we designed an experiment to simultaneously co-deliver the FRET probe ODN$_{HT}$ and mRNA encoding the expression of luciferase (mRNA–Luc) in PC3 cells. We first performed the co-transfection in PC3 cells using the cationic lipid complexes (ODN$_{HT}$–mRNA–lipofectamine, 10 nM ODN$_{HT}$, 1 μg mRNA). The intracellular FRET spectral profiles of ODN$_{HT}$ released in the cytosol were acquired by confocal microscopy (**Figure 7a**) in live cells after 24 h incubation and used to calculate the average value I_A/I_D. The result shown in Figure 7c (FRET 0.69 ± 0.19) indicates the endosomal escape of the ODN$_{HT}$ and subsequent binding to the cytosolic target. After tracking the endosomal escape of the FRET probe, the same cells, treated with ODN$_{HT}$–mRNA–lipofectamine, were used to estimate the expression of luciferase. The mRNA-Luc transfection efficiency was estimated by measuring the luciferase luminescent signal. The co-delivery of mRNA (Figure 7d) resulted in comparable luciferase expression when compared to the control mRNA–lipofectamine (495 ± 32 vs 429 ± 53). From these results, we can infer that, when using a cationic lipid-based carrier, the effective endosomal escape of nucleic acids correlates well with the efficient gene expression.

A similar set of experiments was conducted to evaluate the ability of PG$_{EDA}$ NPs to transfect PC3 cells with ODN$_{HT}$ and mRNA-Luc. The co-delivery of ODN$_{HT}$ (50 nM) and mRNA-Luc (1 μg) was performed using ODN$_{HT}$–mRNA–PG$_{EDA}$ NCs. First, the FRET signal was analyzed by confocal imaging (Figure 7b). The analysis of images revealed the average value I_A/I_D to be lower than 1 (FRET 0.75 ± 0.02), indicating that endosomal escape of the NCs occurred (Figure 7c). Importantly, the co-formulation of nucleic acids did not impair the FRET activity recorded for the NCs when compared to the single delivery of ODN$_{HT}$ using PG$_{EDA}$ (FRET 0.99 ± 0.04).

Despite the variation obtained for the luminescence measurements, increased luciferase activity, up to 30x higher than the untreated control cells, could be detected for the most efficient transfection (Figure 7d). The significant expression of luciferase after transfection with ODN$_{HT}$–mRNA–PG$_{EDA}$ NCs indicates that PG$_{EDA}$ NPs can be used for loading and intracellular co-delivery of nucleic acids with both low and high molecular weights. As the endosomal escape efficiency of ODN$_{HT}$–mRNA–lipofectamine and ODN$_{HT}$–mRNA–PG$_{EDA}$ NCs appear similar (Figure 7c), the lower gene expression observed upon transfection with PG$_{EDA}$ NPs can be likely attributed to the slow or inefficient unpacking of mRNA from NPs in the cytosol. Studies are currently being conducted to optimize the functional design of PG NP by tuning

the stability of PG_{EDA} NPs-mRNA complexes. Collectively, these results show that the triplex-forming oligonucleotide probe can be co-formulated into lipid- and polymer- based nanoparticles along with mRNA allowing the simultaneous correlation of endosomal escape properties of nanoparticles and gene expression efficiency.

3. Conclusion

We designed and validated a stable and bioactive triplex-forming oligonucleotide that served as an intracellular FRET sensor upon binding to NF-κB in live cells. The triplex-forming oligonucleotide was used as a probe and cargo molecule for studying the complex formation (via electrostatic interactions) of PG NPs with oligonucleotides. The stability, structure, and morphology of the nanocomplexes were investigated by STORM with nanoscale resolution. The FRET probe and super-resolution imaging enabled tracking of the intracellular pathway and endosomal escape of oligonucleotides carried by both cationic lipid-based and polymer-based nanoparticles. After internalization, PG_{EDA} NPs prevent the degradation of oligonucleotides and facilitate their intracellular trafficking from early to late endosomes within 2 h incubation. While the endosomal escape and cytosolic release of bioactive oligonucleotide molecules require ≥5 h incubation, we found that the complete binding of the oligonucleotide to the cytosolic target protein occurred after 8 h incubation. The kinetics of nucleic acids binding to the intracellular targets is therefore controlled not only by the endosomal escape capability of the carrier but also by the sustained disassembly of the cargo from PG_{EDA} NPs. This study highlights that sustainably sourced PG NPs with controlled chemical and physical properties can be engineered for the effective intracellular and sustained delivery of oligonucleotides. Finally, we have shown that the engineered FRET probe can be co-formulated with mRNA, using both lipid- and polymer- based carriers to simultaneously probe the effective endosomal escape of nucleic acids and gene expression. This allows the identification of the major barrier to the efficient transfer of genes to the cellular targets, which could guide the rational design of innovative gene delivery systems.

4. Experimental Section

Materials: Oligonucleotide DNA sequences of triplex-hairpin NF-κB, 5′-GGGACT(Quasar570)TTCCTTTAGGAAAGTCCCCTTTGCCCT(Quasar 670)−3′ (the binding domain is underlined, the tail is double underlined), purified by high-performance liquid chromatography, was supplied by LGC Biosearch Technologies (Novato, CA, USA). Human recombinant NF-κB p50 was purchased from Cayman Chemical (Ann Arbor, MI, USA). Lipofectamine RNAiMAX transfection reagent, DNAse I, DNAse I buffer, and 100× Halt protease inhibitor cocktail were obtained from Thermo Fischer Scientific (Waltham, MA, USA). PC3 human prostate epithelial cancer cells (CRL-1435) were purchased from the American Type Culture Collection. Dulbecco's phosphate-buffered saline, bovine serum albumin (BSA), EDA, and sodium cyanoborohydride were supplied by Sigma–Aldrich (St. Louis, MO, USA). PG was purchased from Mirexus Biotechnology Inc. (Guelph, Canada). Opti-MEM reduced serum medium was obtained from Life Technologies (Scoresby, Australia). Trypsin and Dulbecco's modified Eagle's medium (DMEM) were purchased from Lonza (Allendale, USA). Fetal bovine serum (FBS) was supplied by Bovogen Biologicals Pty. Ltd. (Keilor East, Victoria, Australia). Rabbit anti-early endosome antigen 1 (EEA-1) and rabbit anti-Rab7 (9367S) monoclonal antibodies were purchased from Cell Signaling Technology. AF488 NHS ester (succinimidyl ester), AF647 NHS ester (succinimidyl ester), LAMP-1, and goat anti-rabbit immunoglobulin G secondary antibody AF488 were purchased from Invitrogen. All chemicals were used without further purification.

Fluorescence Measurements: Steady-state fluorescence emission spectra were acquired on a Horiba FL-322 Fluorolog-3 spectrofluorometer equipped with a 450 W Xenon arc lamp as an excitation source. The excitation wavelength λ_{ex} was set to 520 nm (excitation slit = 5 nm) and the range of acquisition λ = 550–720 nm was set (emission slit = 5 nm). A fluorescence quartz cuvette with a volume of 200 µL was used. All measurements were carried out at 25 or 37 °C. The solutions were annealed at 95 °C for 5 min and allowed to cool to room temperature for 1 h before measurements. The stability of ODN_{HT} probe (5 nM) was monitored at 25 °C in 137 nM NaCl, and 10 nM $MgCl_2$ at different pH ranging from 4–7, by measuring the fluorescence emission of the donor and acceptor at λ_{ex} 520 nm and slit of 5 nm. The melting curves at different pH values were obtained by measuring the fluorescence emissions of the donor and acceptor as a function of temperature from 20 to 84 °C ($\Delta T = 2$ °C) at λ_{ex} 520 nm and slit of 5 nm, in 14 mM NaCl and 10 mM $MgCl_2$.

Intracellular FRET Analysis in Live Cells: For the live cell FRET experiments, 40000 PC3 cells per well were plated on an 8-well Nunc Lab-Tek II chambered coverglass (Life Technologies, Scoresby, Australia) in DMEM supplemented with 10% FBS and allowed to adhere for 24 h. For the cell transfection experiment by ODN_{HT}–lipofectamine (RNAiMAX), the cells were washed with 1× PBS before replacement of DMEM with OPTI-MEM medium. The cells were treated with solutions of ODN_{HT}–lipofectamine at a final ODN_{HT} concentration of 10 nM according to the supplier's protocol. For the cell transfection experiment by ODN_{HT}–PG_{EDA} NCs (ratio 1:36), final ODN_{HT} concentrations of 25 and 50 nM ODN_{HT} were used. After incubation for 2 h at 37 °C and 5% CO_2, the cells were washed three times with 1× PBS, and the medium was replaced. The cells were incubated further for 3, 4, 6, 10, and 22 h in DMEM medium. After each incubation period, the medium was replaced with Leibovitz's medium supplemented with 10% FBS, and the live cells were analyzed by laser scanning confocal microscopy (LSCM; Nikon A1R equipped with a 60 × 1.4 NA oil immersion objective) at λ_{ex} 546 nm (donor excitation), and the images and spectral emission profiles of the donor and acceptor were acquired in range of 560–700 nm. High voltage (gain), offset, and laser power were kept constant during the data acquisition of all samples and controls. Image processing was performed using the NIS-Element confocal software (Nikon). For the intracellular FRET measurements, for each condition, at least 30 cells were analyzed. For cell viability of PC3 cells after incubation for 48 h with ODN_{HT}–PG_{EDA} NCs at different concentrations alamarBlue assay was used.

Potentiometric Titration: To determine the pK_a of PG_{EDA} NP suspension, 3 mL of 10 mg mL^{-1} PG_{EDA} NP suspension was used. The pH of the suspension was adjusted to >10 using NaOH (0.01 N). The suspension was then titrated using HCl solution (0.01 N) and the pH was recorded as a function of the volume of HCl.

Characterization of ODN_{HT}–PG_{EDA} NCs by TEM: For TEM imaging, the sample (10 µL, 10 mg mL^{-1}) was deposited on copper grid for 10 min. The sample was then removed, and the grid was washed with Milli-Q water twice. Then, uranyl acetate (10 µL) was added to the grid for 1 min and washed twice with water. The grid was then air-dried and imaged on a JEOL 1010 transmission electron microscope. Cryo-TEM images were obtained using a TECNAI F30 microscope equipped with a high-angle annular dark-field scanning transmission electron microscopy detector, a Gatan quantum 965 energy filter, and an upper CETA 4 × 4k CMOS camera.

Cell Culture: Human prostate cancer PC3 cells were cultured in DMEM (Lonza, Basel, Switzerland) supplemented with 10% FBS at 37 °C and in 5% CO_2. After reaching 80%–90% confluency, cells were detached using an enzyme-free dissociation buffer (Gibco, Thermo Fisher Scientific) and reseeded in the relevant culture dish.

Binding of ODN_{HT} to NF-κB in Test Tube: The binding of ODN_{HT} to NF-κB was examined by fluorescence emission spectroscopy following incubation of ODN_{HT} with NF-κB p50/p50 homodimer at increasing

concentrations in the range of 0.1–100 nM. Fluorescence gain values (%) were calculated from enhancements in the donor fluorescence intensity (at 570 nm) to the initial fluorescence. Data were analyzed according to the Hill equation[12] (Equation 1):

$$\text{Fluorescence gain } (\%) = \frac{m[\text{NF} - \kappa\text{B}]^n}{K_d^n + [\text{NF} - \kappa\text{B}]^n} \quad (1)$$

where m is maximum fluorescence gain, K_d is the apparent dissociation constant, and n is a coefficient. According to this fitting, K_d is (25 ± 1) nM and n is 2.85, indicating a cooperative binding process. K_S value was estimated assuming that the ODN_{HT} exists in two discrete conformations, (triplex, and duplex states), each associated with a distinct FRET value, and the FRET efficiency at the equilibrium arises from the linear combination of these two extreme energy transfer conditions.

The FRET efficiency ($FRET_{solution}$) in solution was calculated using Equation (2):

$$FRET_{solution}\ [\%] = \frac{I_{max} - I_{DA}}{I_{max}} \times 100\ \% \quad (2)$$

where I_{DA} is the donor fluorescence intensity measured at the equilibrium and after binding to NF-κB. I_{max} is the maximum donor fluorescence emission. I_{max} was measured by treating the ODN_{HT} with DNase I, which resulted in degradation of the probe and complete loss of energy transfer between the fluorophore pair. In the duplex-bound state, the measured FRET value was 17%. At the equilibrium condition, the experimental FRET value was 70%. By assuming that in the triplex conformation, the donor was quenched by both contact and FRET effects (i.e., FRET triplex = 100%) a Ks of 0.6 at 37 °C was estimated.

FCS Measurements: FCS measurements were performed using a MicroTime PicoQuant system combined with a Nikon A1R confocal microscope equipped with either a 40 × 1.1 NA water immersion objective (measurements in solution) or a 60 × 1.4 NA oil immersion objective (measurements in cells). The ODN_{HT} in solution or inside cells was excited using a 561 nm laser and signals were detected using a 600/50 bandpass filter. The confocal volume (0.7 fL) was calibrated using AF555 as a reference, and D was calculated using the D of AF555 as a standard (300 $\mu m^2\ s^{-1}$). The autocorrelation curves were best fitted with a Brownian diffusion model including triplet dynamic and one component using the SymPhoTime 64 software. For each condition in the solution, 20 measurements were performed. FCS was also used to determine the diffusional properties of ODN_{HT} (50 nM) after lipofectamine-mediated transfection in live PC3 cells in accordance with a previously reported protocol.[5a]

Synthesis and Labeling of PG_{EDA} NPs: PG (200 mg, equivalent to 1.2 mmol of glucose monomers) was dissolved in acetic buffer (5 mL, 0.6 M; pH 5.5) with stirring. To this, sodium periodate (42 mg, 0.24 mmol) was added for oxidation of 1, 2 diols in the dark. After 2 h, EDA (72 mg, 1.2 mmol) was added followed by sodium cyanoborohydride (10 eq.), and the mixture was stirred overnight. The product was purified by dialysis (molecular weight cutoff (MWCO) 14 kDa) against Milli-Q water for 3 days (water was replaced six times) and freeze-dried. The yield of the reaction was ≈90%. The degree of substitution was determined by ^{1}H NMR spectroscopy on an Agilent DD2 500 MHz NMR spectrometer at 80 °C. Samples were dissolved in D_2O with residual solvent signal (δ_H 4.79) used as an internal reference. An aqueous suspension of PG_{EDA} NPs (10 mg mL^{-1}) was prepared in 0.1 N $NaHCO_3$ buffer pH 8–9. AF647 NHS (20 µL, 1 mg mL^{-1}) was added to the solution at room temperature and incubated overnight in the dark under continuous shaking. The suspension was then purified using a NAP-10 filter column and dialysis (MWCO 14 kDa) and freeze-dried.

Complexation Between Cationic PG_{EDA} and ODN_{HT}: To prepare complexes between cationic PG_{EDA} NPs and ODN_{HT}, a solution of ODN_{HT} (200 nM) in NaCl (5 mM) was prepared and different aliquots of PG_{EDA} NPs (1 mg mL^{-1}) were added to obtain different weight ratios of ODN_{HT}-to-PG_{EDA} NP ranging from 1:0.3 to 1:36. The mixture was vortexed for 10 s and incubated at room temperature for 20 min. The size and ζ-potential of the complexes were then determined using a Malvern Zetasizer. The effective loading of ODN_{HT} was determined through fluorescence measurements at λ_{ex} 520 nm after filtration by spin-column (MWCO 100 kDa).

Characterization of ODN_{HT}–PG_{EDA} NCs by STORM: For STORM analysis, ODN_{HT}–PG_{EDA} NCs were prepared as described above at different ODN_{HT}-to-PG_{EDA} NP ratios, i.e., 1:4.5, 1:9, 1:18, and 1:36 in 5 mM NaCl while the concentration of ODN_{HT} was kept constant at 200 nM. ODN_{HT}–PG_{EDA} NCs or PG_{EDA} NPs were deposited on a glass slide. After 30 min of incubation at 25 °C, unbound molecules and nano complexes were washed away with freshly prepared, standard imaging buffer with cysteamine. STORM images were acquired using a Nikon N-STORM system equipped with a Nikon 100 × 1.4 NA oil immersion objective. The focus and the TIRF imaging angle were adjusted to obtain a high signal-to-noise ratio. A 647 nm laser was used for excitation of the fluorophores. All time lapses were recorded within a 256 pixels × 256 pixels region using an EMCCD camera. For each image, 4000 frames were acquired sequentially using full laser power. STORM images were first processed with the STORM module of the NIS Elements Nikon software, where drift correction was performed, and a list of particle localizations was obtained by Gaussian fitting of the fluorescence spots of blinking dyes. Blinking events that were detected in ≤5 consecutive frames were counted as single molecules, whereas events detected in more than 5 consecutive frames were discarded (maximum trace length 5). The list of localizations was exported as a text file and analyzed using a Python clustering analysis script where the localizations were clustered using a kernel density estimation with a bandwidth of 50 nm. An ellipse was fitted to the obtained clusters with a minimum of 10 localizations and a maximum elongation factor of 1.5 (ratio of long and short axes of the ellipse). Then, the circles containing 90% of detected spots in the cluster were fitted, allowing for the determination of the particle size distribution and number of localizations.

Intracellular Trafficking and Colocalization Studies in Fixed Cells by LSCM and STORM: For intracellular trafficking studies, ≈30000 PC3 cells were seeded on 8-well Lab-Tek chamber slides, followed by the addition of culture medium (0.5 mL) and incubation overnight. The cells were then incubated with ODN_{HT}–PG_{EDA} NCs (ratio 1:36) containing 50 nM ODN_{HT} for 2 h, washed with 1 × PBS, and further incubated for 3, 7, 22, and 46 h in DMEM supplemented with 10% FBS. After each time point, the cells were fixed, permeabilized, blocked with 2.5% BSA, and incubated with primary antibodies (2 µg mL^{-1}), specific for early endosome, late endosome, and lysosome staining by EEA-1 monoclonal antibody, rabbit-Rab7 monoclonal antibody, or rabbit LAMP-1 for 2.5 h, at 25 °C, respectively. Then the cells were washed three times with 1×PBS and further incubated for 1.5 h with goat anti-rabbit immunoglobulin G secondary antibody AF488 conjugate (2 mg mL^{-1} at 25 °C). Confocal laser scanning microscopy images of NF-κB protein and ODN_{HT}, after 5 and 24 h transfection by ODN_{HT}–PG_{EDA} NCs (concentration of ODN_{HT} = 50 nM) were acquired after immunostaining with AF488-labeled anti-NF-κB p50 antibody. The cells were imaged with a Nikon A1R confocal microscope with a 60 × 1.4 NA oil immersion objective. Pearson coefficient (R) was obtained using the ImageJ software. Multicolor STORM images of NF-κB protein and ODN_{HT} after 24 h transfection by ODN_{HT}–PG_{EDA} NCs were acquired on fixed and permeabilized cells. The cells were incubated for 1 h with rabbit anti-NF-κB p50 primary antibody (2 µg mL^{-1}) followed by washing three times with PBS and further incubation with the dual-labeled AF488/AF647 goat anti-rabbit secondary antibody. The dual-labeled secondary antibody was prepared as follows: secondary antibody AF488 (50 µL; 2 mg mL^{-1} in PBS) was mixed with $NaHCO_3$ (50 µL, 0.1 M) and AF647 (10 µL; activator dye/reporter dye = 2:1). The reaction proceeded for 30 min at 25 °C in the dark while stirring on a shaking platform. The reaction volume was adjusted to 0.5 mL. Then, the antibody was purified using a NAP-5 gel filtration column equilibrated in PBS. STORM images were acquired using a Nikon N-STORM system configured for TIRF imaging using a Nikon 100 × 1.4 NA oil immersion objective and passed through a quad-band pass dichroic filter. The perfect focus system and TIRF angle were adjusted and tuned to maximize the signal-to-noise ratio. The dual-labeled (AF488- and AF647-labeled) antibody and ODN_{HT} (Quasar570, Quasar670) were excited by 488, 561, and 647 nm laser. As the reporter dyes on the secondary antibody (AF647) and ODN_{HT} (Quasar670) exhibit similar photophysical properties and

quantum yields (0.33), the detection efficiency was assumed to be the same for both molecules. To qualitatively verify the colocalization between NF-κB and ODN_{HT} by imaging for each experimental condition, ≈30 cells were analyzed.

Co-Delivery of ODN_{HT} and mRNA to PC3 Cells: For the FRET and luciferase expression experiments, ≈40000 PC3 cells were seeded on an 8-well Nunc Lab-Tek II chambered coverglass (Life Technologies, Scoresby, Australia) in DMEM supplemented with 10% FBS and allowed to adhere for 24 h. For the cell transfection experiments using ODN_{HT}–mRNA–lipofectamine (RNAiMAX), the cells were washed with 1 × PBS before replacement of DMEM with OPTI-MEM medium. The cells were treated with solutions of ODN_{HT}–mRNA–lipofectamine at a final ODN_{HT} concentration of 10 nM according to the supplier's protocol and 1 µg of mRNA encoding luciferase per well. For the cell transfection experiment with ODN_{HT}–mRNA–PG_{EDA} NCs (ratio ODN_{HT}:PG_{EDA} 1:36), a final ODN_{HT} concentration of 50 nM and 1 µg of mRNA encoding luciferase per well were used. After incubation for 4 h at 37 °C and 5% CO_2, the cells were washed three times with 1 × PBS, and the medium was replaced. The cells were incubated for a further 20 h in DMEM medium containing 10% FBS. After the 24 h incubation period, the live cells were analyzed by laser scanning confocal microscopy (LSCM; Nikon A1R equipped with a 60 × 1.4NA oil immersion objective) at λ_{ex} 546 nm (donor excitation), and the images and spectral emission profiles of the donor and acceptor were acquired in range of 560–700 nm. High voltage (gain), offset, and laser power were kept constant during the data acquisition of all samples and controls. Image processing was performed using the NIS-Element confocal software (Nikon). For the intracellular FRET measurements, for each condition, at least 30 cells were analyzed. For mRNA transfection efficiency evaluation, luciferase expression was estimated using the ONE-Glo EX Luciferase Assay System (Promega, E8130) according to the manufacturer's procedure.

Statistical Analysis: All results are shown as mean ± s.d. The statistical significance and *p* values were analyzed with Minitab 18 (Minitab LCC, Pennsylvania, USA), using one-way analysis of variance (ANOVA) with 95% confidence interval and Tukey's pairwise comparison.

Supporting Information

Supporting Information is available from the Wiley Online Library or from the author.

Acknowledgements

F.Cavalieri acknowledges the award of an RMIT Vice Chancellor Senior Research Fellowship and F.Caruso acknowledges the award of a National Health and Medical Research Council Leadership Fellowship (GNT2016732). This work was supported by the Australian Research Council under a Discovery Project scheme (F. Cavalieri, C.C.-J., and N.M., DP210101792). This work received funding from the European Union's Horizon 2020 research and innovation program under the Marie Skłodowska-Curie grant agreement no. 690901 ("NANOSUPREMI"). This work was performed in part at the Materials Characterization and Fabrication Platform (MCFP) and Bio21 Ian Holmes Imaging Center at The University of Melbourne. The authors acknowledge Haiyan Zhun and Domitilla Vanni for providing help with TEM and NMR measurements.

Conflict of Interest

The authors declare no conflict of interest.

Author Contributions

S.K.B. and L.M. contributed equally to this work. The manuscript was written through the contributions of all authors. All authors have approved the final version of the manuscript.

Data Availability Statement

The data that support the findings of this study are available from the corresponding author upon reasonable request.

Keywords

endosomal escape, phytoglycogen, super-resolution microscopy, triplex-forming oligonucleotide

Received: September 16, 2023
Revised: December 22, 2023
Published online:

[1] J. P. Bost, H. Barriga, M. N. Holme, A. Gallud, M. Maugeri, D. Gupta, T. Lehto, H. Valadi, E. K. Esbjörner, M. M. Stevens, S. El-Andaloussi, *ACS Nano* **2021**, *15*, 13993.
[2] a) Y. Wang, L. Miao, A. Satterlee, L. Huang, *Adv. Drug Delivery Rev.* **2015**, *87*, 68; b) D. C. Luther, R. Huang, T. Jeon, X. Zhang, Y.-W. Lee, H. Nagaraj, V. M. Rotello, *Adv. Drug Delivery Rev.* **2020**, *156*, 188.
[3] a) I. M. S. Degors, C. Wang, Z. U. Rehman, I. S. Zuhorn, *Acc. Chem. Res.* **2019**, *52*, 1750; b) D. Habrant, P. Peuziat, T. Colombani, L. Dallet, J. Gehin, E. Goudeau, B. Evrard, O. Lambert, T. Haudebourg, B. Pitard, *J. Med. Chem.* **2016**, *59*, 3046.
[4] a) T. Andrian, R. Riera, S. Pujals, L. Albertazzi, *Nanoscale Adv.* **2021**, *3*, 10; b) Y. Yamaoki, T. Nagata, T. Sakamoto, M. Katahira, *Biophys. Physicobiol.* **2020**, *17*, 36.
[5] a) A. Glab, A. Bertucci, F. Martino, M. Wojnilowicz, A. Amodio, M. Venanzi, F. Ricci, G. Forte, F. Caruso, F. Cavalieri, *Nanoscale* **2020**, *12*, 15402; b) A. Bertucci, J. Guo, N. Oppmann, A. Glab, F. Ricci, F. Caruso, F. Cavalieri, *Nanoscale* **2018**, *10*, 2034; c) M. Wojnilowicz, A. Glab, A. Bertucci, F. Caruso, F. Cavalieri, *ACS Nano* **2018**, *13*, 187; d) P. Paramasivam, C. Franke, M. Stöter, A. Höijer, S. Bartesaghi, A. Sabirsh, L. Lindfors, M. Y. Arteta, A. Dahlén, A. Bak, S. Andersson, Y. Kalaidzidis, M. Bickle, M. Zerial, *J. Cell Biol.* **2022**, *221*, 202110137; e) R. Riera, J. Tauler, N. Feiner-Gracia, S. Borrós, C. Fornaguera, L. Albertazzi, *ChemMedChem* **2022**, *17*, 202100633; f) R. Riera, N. Feiner-Gracia, C. Fornaguera, A. Cascante, S. Borrós, L. Albertazzi, *Nanoscale* **2019**, *11*, 17869; g) N. Feiner-Gracia, R. A. Olea, R. Fitzner, N. El Boujnouni, A. H. Van Asbeck, R. Brock, L. Albertazzi, *Nano Lett.* **2019**, *19*, 2784.
[6] S. Schmidt, M. J. W. Adjobo-Hermans, R. Wallbrecher, W. P. R. Verdurmen, P. H. M. Bovée-Geurts, J. Van Oostrum, F. Milletti, T. Enderle, R. Brock, *Angew. Chem. Int. Ed.* **2015**, *54*, 15105.
[7] Y. Jiang, Q. Lu, Y. Wang, E. Xu, A. Ho, P. Singh, Y. Wang, Z. Jiang, F. Yang, G. T. Tietjen, P. Cresswell, W. M. Saltzman, *Nano Lett.* **2020**, *20*, 1117.
[8] S. L. Y. Teo, J. J. Rennick, D. Yuen, H. Al-Wassiti, A. P. R. Johnston, C. W. Pouton, *Nat. Commun.* **2021**, *12*, 3721.
[9] R. Xu, S. K. Bhangu, K. C. Sourris, D. Vanni, M.-A. Sani, J. A. Karas, K. Alt, B. Niego, A. Ale, Q. A. Besford, B. Dyett, J. Patrick, I. Carmichael, J. E. Shaw, F. Caruso, M. E. Cooper, C. E. Hagemeyer, F. Cavalieri, *Adv. Mater.* **2023**, *35*, 2210392.
[10] J. Xue, J. Inzero, Q. Hu, T. Wang, Wusigale, Y. Luo, *Food Hydrocolloids* **2019**, *95*, 256.
[11] A. Vallée-Bélisle, F. Ricci, K. W. Plaxco, *Proc. Natl. Acad. Sci.* **2009**, *106*, 13802.
[12] D. A. Rusling, P. A. Rachwal, T. Brown, K. R. Fox, *Biophys. Chem.* **2009**, *145*, 105.

[13] a) H. D. Heck, *J. Am. Chem. Soc.* **1971**, *93*, 23. b) C. B. Phelps, L. L. Sengchanthalangsy, S. Malek, G. Ghosh, *J. Biol. Chem.* **2000**, *275*, 24392.
[14] J.-I. Lee, G. J. Burckart, *J. Clin. Pharmacol.* **1998**, *38*, 981.
[15] a) J. Charostad, M. Nakhaie, A. Dehghani, E. Faghihloo, *Infect. Agents Cancer* **2020**, *15*, 62; b) C. Guijarro, J. Egido, *Kidney Int.* **2001**, *59*, 415; c) M. Karin, Y. Cao, F. R. Greten, Z.-W. Li, *Nat. Rev. Cancer* **2002**, *2*, 301; d) R. R. Rasmi, K. M. Sakthivel, C. Guruvayoorappan, *Biomed. Pharmacother.* **2020**, *130*, 110569.
[16] J.-L. Putaux, A. Buléon, R. Borsali, H. Chanzy, *Int. J. Biol. Macromol.* **1999**, *26*, 145.
[17] A. Radziwon, S. K. Bhangu, S. Fernandes, C. Cortez-Jugo, R. De Rose, B. Dyett, M. Wojnilowicz, P. Laznickova, J. Fric, G. Forte, F. Caruso, F. Cavalieri, *Nanoscale* **2022**, *14*, 3452.
[18] J. D. Nickels, J. Atkinson, E. Papp-Szabo, C. Stanley, S. O. Diallo, S. Perticaroli, B. Baylis, P. Mahon, G. Ehlers, J. Katsaras, J. R. Dutcher, *Biomacromolecules* **2016**, *17*, 735.